Nano Today 60 (2025) 102561

Contents lists available at ScienceDirect

Nano Today

journal homepage: www.elsevier.com/locate/nanotoday

Blue phosphorescent solid supramolecular assemblies between hydroxypropyl-β-cyclodextrin and triazine derivatives for achieving multicolor delayed fluorescence

Xuan Zhao, Xiaolu Zhou, Qingwen Cheng, Yu Liu *

College of Chemistry, State Key Laboratory of Elemento-Organic Chemistry, Nankai University, Tianjin 300071, PR China

ARTICLE INFO

Keywords:
Blue phosphorescence
Supramolecular assembly
Triazine derivatives
Hydroxypropyl-β-cyclodextrin
Multicolor delayed fluorescence

ABSTRACT

Highly efficient blue phosphorescent solid supramolecular assemblies are constructed by three triazine derivatives with different carboxylate substitution positions (TAB, TAC and TAD), hydroxypropyl-β-cyclodextrin (HPCD) and polyvinyl alcohol (PVA). The encapsulation of HPCD to TAB/C/D effectively promotes phosphorescence lifetimes and quantum yields of the guests by the host-guest interaction and hydrogen bonds suppressing the nonradiative decays. Impressively, TAD-HPCD/PVA with blue phosphorescence boasts an ultrahigh phosphorescence quantum yield (Φ_P) of 71.65 %. By further separately doping with fluorescent dyes Fluorescein sodium, Rhodamine B and Sulfo-Cyanine5, supramolecular polymeric films with water responsiveness, regulable lifetimes and multicolor delayed fluorescence are obtained via triplet-to-singlet and singlet-to-singlet Förster resonance energy transfer. Polymeric phosphorescence supramolecular materials mediated by HPCD are desirable for optical anti-counterfeiting patterns and information encryption.

Introduction

Supramolecular cascade assembly based on host-guest complexation can not only induce the fluorescence/phosphorescence emission of the guest or host but also achieve effective cascade energy transfer [1–3], which is a hot research area because it is widely applied in targeted cell imaging [4–6], molecular machines [7–9], multicolor emission [10–12] and information anti-counterfeiting [13,14]. When the functional guest molecule is encapsulated in the hydrophobic cavity of macrocyclic molecules such as cucurbituril [15,16] and cyclodextrin [17,18], the spatial confinement effect can significantly induce or enhance its phosphorescence emission [19]. In particular, functional cyclodextrin host-guest complexes can further cascade assembly with energy acceptors via multivalent interactions leading to phosphorescence resonance energy transfer (PRET) for achieving multicolor delayed fluorescence [20–22]. Thus, many studies have been reported on cyclodextrin-confined room temperature phosphorescence (RTP) supramolecular assemblies. For example, Li et al. reported that the β-cyclodextrin (β-CD) host induced obvious chirality of p-biphenylboronic acid guest through macrocyclic encapsulation and hydrogen bonding interactions, as well as promoted the RTP emission in aqueous solution, and then further realized the tuning of the afterglows from blue to pink after adding Rhodamine B dye through PRET [23]. Recently, Liu et al. proposed a thermally responsive deep-blue RTP solid polyvinyl alcohol (PVA)-matrix film based on the β-CD encapsulating terephthalic acid, and heating can disassemble the host-guest complex to display the green phosphorescence emission of the original guest [24]. Notably, the PVA polymer matrix can not only avoid emission quenching caused by chromophore aggregation, but also improve the flexibility and processability of amorphous solid supramolecular assembly [25–27]. Tang et al. fabricated a series of blue RTP materials by doping indolocarbazole isomers into the PVA matrix, among which an excellent RTP property with the highest quantum yield of 44.1 % was achieved due to the strong electrostatic attraction generated by the synergistic double hydrogen bonds between the isomer 11,12-dihydroindolo[2,3-*a*]carbazole and PVA, and then mixed Fluo/Rh6G/RhB fluorescent dyes to achieve color-tunable and time-dependent luminescence [28]. However, blue RTP supramolecular materials with quantum yields higher than 50 % in PVA-matrix are rarely reported, to the best of our knowledge. Therefore, it is highly desirable to propose a new strategy to fabricate a facile, efficient and ultra-bright blue phosphorescence system.

Herein, we wish to report blue phosphorescent solid supramolecular assemblies with high quantum yield constructed by three triazine derivatives modified by carboxy-phenylamino groups, hydroxypropyl-

* Corresponding author.
E-mail address: yuliu@nankai.edu.cn (Y. Liu).

https://doi.org/10.1016/j.nantod.2024.102561
Received 26 August 2024; Received in revised form 3 November 2024; Accepted 21 November 2024
Available online 24 November 2024

β-cyclodextrin (HPCD) and PVA, which can further coassemble with fluorescence dyes for achieving multicolor delayed fluorescence. Due to the influence of different substitution positions of the carboxyl group on the intramolecular hydrogen bonding (IHB), steric hindrance effect and the host-guest binding, the supramolecular assemblies of para-/meta-/ortho-carboxy-phenylamino triazine derivatives (TAB, TAC and TAD) and HPCD display obviously different phosphorescence emission behaviors. Apparently, the TAD-HPCD supramolecular assembly gives the highest phosphorescence quantum yield (Φ_P) of 52.75 % benefitting from the macrocyclic confinement and multiple hydrogen bonding interactions. Moreover, the secondary assembly of TAD-HPCD nanoparticles and PVA matrix can provide a more rigid microenvironment to restrict the chromophore motion and inhibit non-radiative transition, ulteriorly extending the ultra-bright blue emission with Φ_P up to 71.65 %. This is an ultrahigh blue phosphorescent quantum yield in the PVA system in current reports. TAB-HPCD/PVA and TAC-HPCD/PVA also exhibit blue phosphorescence with the quantum yields of 29.87 % and 9.54 % at ambient conditions. The ultralong lifetimes of TAD-HPCD/PVA, TAC-HPCD/PVA and TAB-HPCD/PVA are 102.99 ms, 126.06 ms and 526.03 ms, respectively, which are regarded as stable and ideal phosphorescence energy transfer platforms to realize multicolor delayed fluorescence. The delayed fluorescence peaks at 520 nm or 590 nm were observed by doping commercial dyes Fluorescein sodium (Flu) or Rhodamine B (RhB) into supramolecular films via triplet-to-singlet Förster resonance energy transfer (TS-FRET). Furthermore, by adding the secondary dye Sulfo-Cyanine5 (Cy5) into the above systems, the singlet-to-singlet Förster resonance energy transfer (SS-FRET) process took place from RhB to Cy5 with the highest energy transfer efficiency of 90.70 % (Scheme 1). The macrocycle-confined solid supramolecular PVA films can produce not only highly efficient blue phosphorescence with water responsiveness but also multicolor delayed fluorescence with tunable lifetimes, which provides sufficient conditions for information encryption and colored drawing.

Results and discussion

2,4,6-tri ((p-carboxyphenyl) amino)-1,3,5-triazine (TAB), 2,4,6-tri ((m-carboxyphenyl) amino)-1,3,5-triazine (TAC) and 2,4,6-tri ((o-carboxyphenyl) amino)-1,3,5-triazine (TAD) were synthesized as the guests and their structures were determined by hydrogen nucleus magnetic resonance (^{1}H NMR) spectroscopy, carbon nuclear magnetic resonance (^{13}C NMR) spectroscopy and high-resolution mass spectrometry (Scheme S1; Fig. S1-S6). The guest molecules contain not only the triazine moiety as a phosphorescence-active unit [29,30] but also multiple N atoms and carboxyl groups promoting the n-π* leaps and spin-orbit coupling (SOC), which can construct H-bonding cross-linked networks with the hosts and polymer matrix to efficiently suppress non-radiative decay channels [31–34]. Considering the excellent water solubility and hydrophobic cavity, HPCD was chosen as the host molecule that could bind with guest molecules to induce or promote the phosphorescence emission via the macrocyclic confinement effect [35]. In our work, we prepared the TAD-HPCD supramolecular assembly by sonicating and lyophilizing an aqueous mixture with a molar ratio of 1:3, and demonstrated that the host-guest binding of HPCD to TAD could realize an efficient blue phosphorescence due to the spatial confinement restricting chromophores. TAB-HPCD and TAC-HPCD with para-/meta-carboxy groups were also prepared and investigated their luminescence properties and host-guest binding behaviors under ambient conditions. The X-ray powder diffraction (XRD) experiment confirmed that these three freeze-dried powders were in an amorphous state (Fig. S7).

Luminescence behaviors of solid supramolecular assembly

The steady-state PL and phosphorescence spectra of TAD-HPCD powder were performed and the emission peak curves almost overlapped presenting blue emission at 430 nm (Fig. 1a). The fluorescence emission band at 370 nm in the PL spectrum recorded a lifetime of 4.10 ns, and the time-resolved decay curve monitored at 430 nm had a lifetime of 4.11 ms (Fig. 1f; Fig. S8). The CIE coordinate chart in Fig. 1d also revealed that the phosphorescence emission of TAD-HPCD was located in the blue region at the coordinates (x: 0.16, y: 0.16). However, freeze-dried TAD powder without HPCD exhibited very weak RTP with a lifetime of 3.71 μs (Fig. S9, S10). This could be the cause of aggregation-

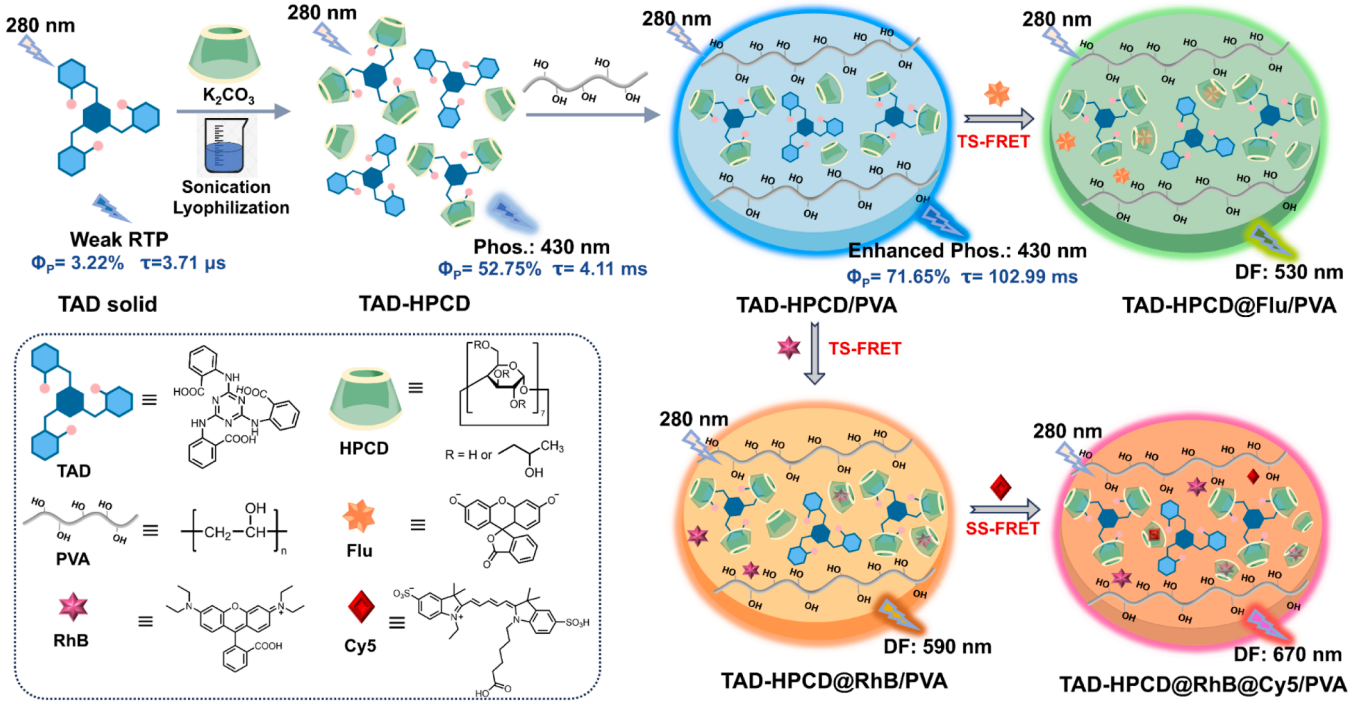

Scheme 1. Schematic illustration of the multilevel assembly mechanism of TAD-HPCD/PVA supramolecular film, multicolor TS-FRET and SS-FRET systems.

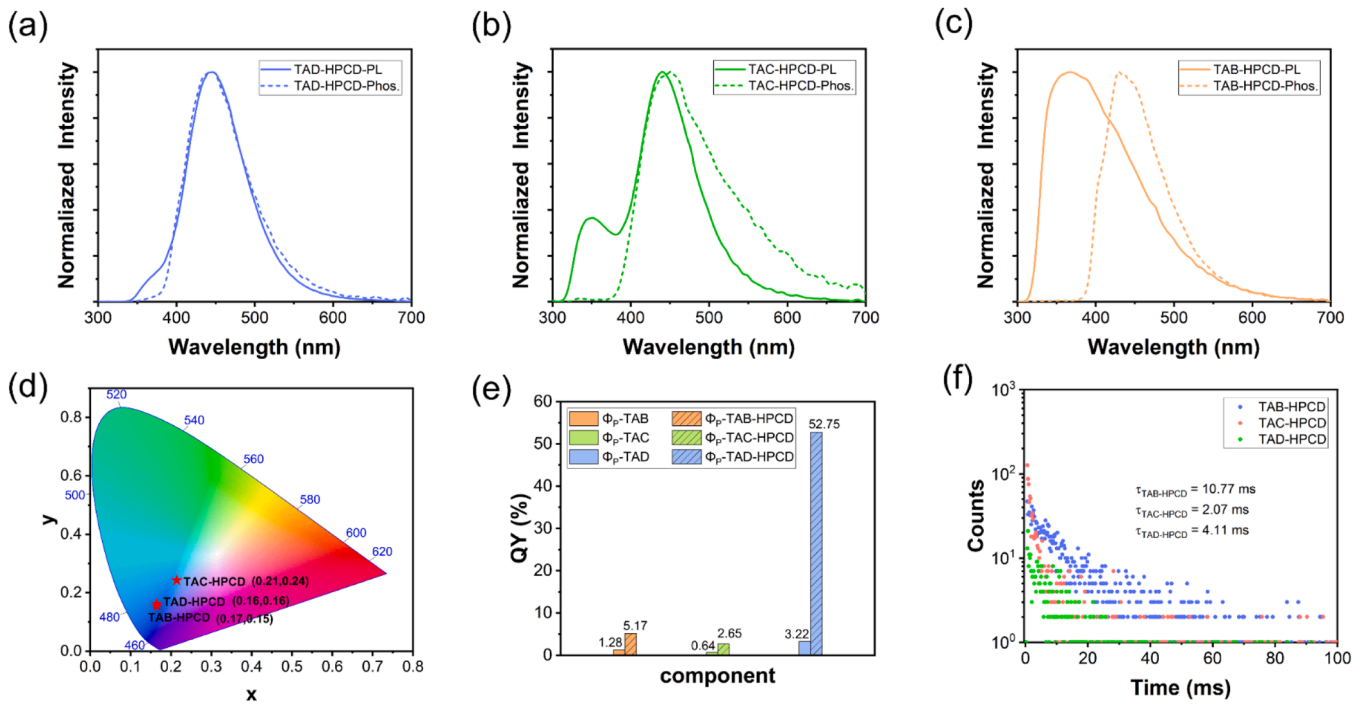

Fig. 1. Normalized steady-state PL (solid line) and phosphorescence (dotted line) spectra of (a) TAD-HPCD, (b) TAC-HPCD and (c) TAB-HPCD powders (λ_{ex}=280 nm, delayed time=100 μs); (d) CIE 1931 chromaticity diagram of TAB/C/D-HPCD solids according to (a, b, c); (e) Phosphorescent quantum yields of six solids; (f) Time-resolved decay spectra of TAB/C/D-HPCD assemblies ([TAB/C/D]:[HPCD]=1:3, recorded at 430 nm).

induced phosphorescence quenching. The phosphorescent quantum yield of TAD-HPCD supramolecular assembly was 52.75 %, which was 16 times higher than that of TAD (Φ_P=3.22 %). As expected, compared with the original TAB (Φ_P=1.28 %) and TAC (Φ_P=0.64 %) powders, TAB-HPCD and TAC-HPCD also promoted the blue phosphorescence emission, and the phosphorescent quantum yields were increased to 5.17 % and 2.65 %, respectively (Fig. 1b, c, e; Table S1). Thus, HPCD played an important spatial confinement role in this amorphous organic blue RTP system.

Considering that the abundant hydroxyl groups of PVA can form a

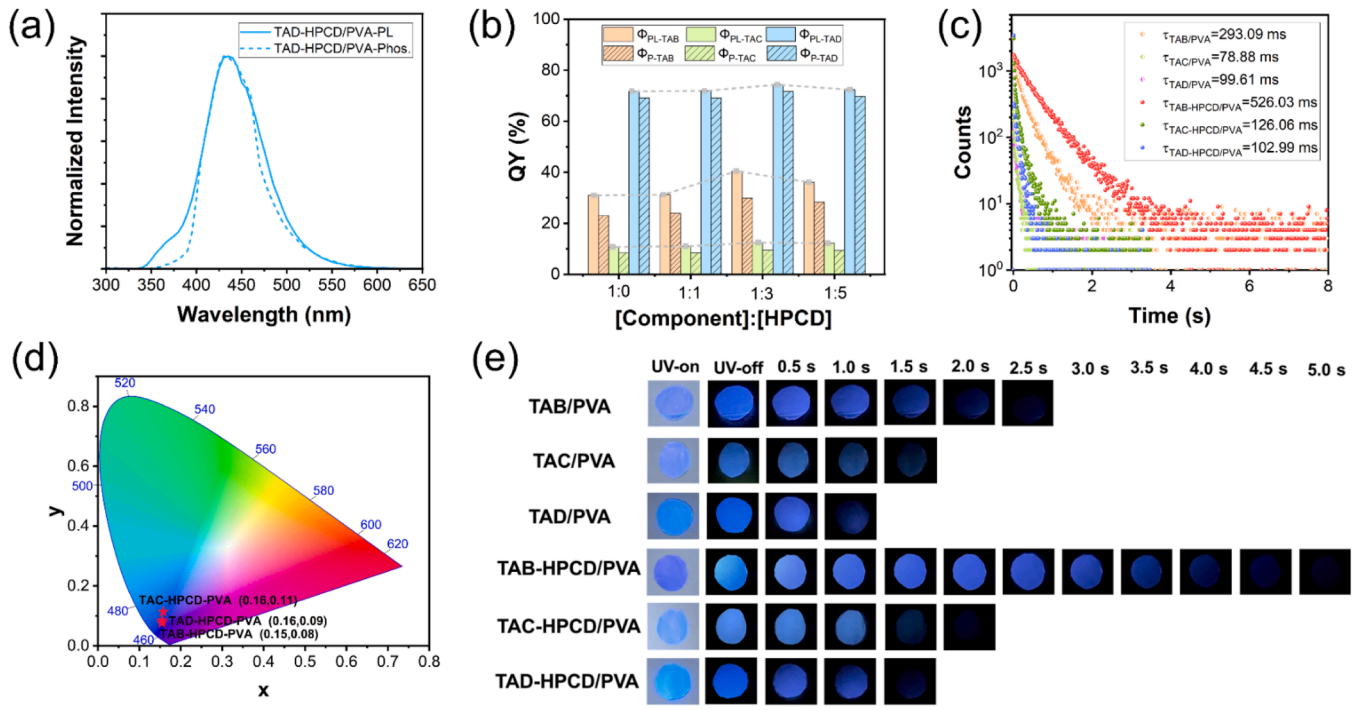

Fig. 2. (a) Normalized steady-state PL and phosphorescence spectra of TAD-HPCD/PVA ([TAD]:[HPCD]=1:3, m_{TAD}:m_{PVA}=1:200, λ_{ex}=280 nm, delayed time=100 μs); (b) Histogram of quantum yields of TAB/C/D-HPCD/PVA at different host-guest molar ratios; (c) Time-resolved decay spectra of six PVA films; (d) CIE 1931 chromaticity diagram of TAB/C/D-HPCD/PVA films according to their phosphorescence spectra; (e) The afterglow photographs of six PVA films after the 300 nm UV lamp was turned off.

rigid hydrogen bond network to restrict the motion of TAD [36–38], we further prepared TAD/PVA films with different doping mass ratios from 0.01 wt% to 10 wt%. According to the trend of emission spectra and phosphorescent quantum yields, the best doping concentration is 0.5 wt % (Fig. S11, S12; Table S2). It is worth noting that adding HPCD to the TAD/PVA film can further improve the phosphorescence lifetime and quantum yield. When the doping molar ratio of TAD and HPCD was 1:3, the TAD-HPCD supramolecular nanoparticles were doped into PVA. The prepared 0.5 wt%-TAD-HPCD/PVA presented excellent RTP property with an ultralong lifetime of 102.99 ms and the highest phosphorescence quantum yield of 71.65 % (Fig. 2a, b, c; Table S3). As far as we know, it is the highest Φ_P ever recorded in blue phosphorescent PVA films (Table S4). The optimal luminescence performance was achieved when the mass ratio of TAD: PVA is 1:200 and the molar ratio of TAD: HPCD is 1:3. The phosphorescence emission of TAD-HPCD/PVA was located at the coordinates (x: 0.16, y: 0.09) in the deep-blue region through its CIE coordinate chart, which was consistent with its afterglow photograph in Fig. 2d, e. In the control experiment, doping TAB and TAC into PVA produced dual-emission of fluorescence and phosphorescence, and the luminescence performance was best when the doping ratio was also 0.5 wt% (Fig. S11). When the molar ratio of TAB or TAC:HPCD reached 1:3, the phosphorescent quantum yields of 0.5 wt %-TAB-HPCD/PVA and 0.5 wt%-TAC-HPCD/PVA were measured at 29.87 % and 9.54 %, respectively, which were lower than that of 0.5 wt %-TAD-HPCD/PVA. Similarly, the host molecule HPCD also significantly lengthened the phosphorescent lifetimes of 0.5 wt%-TAB/PVA and 0.5 wt%-TAC/PVA up to 526.03 ms and 126.06 ms, respectively, which might be due to the host-guest binding effect (Fig. S13, S14). TAB/C/D-HPCD/PVA films exhibit the highest quantum yield compared to α, β, γ-cyclodextrin (α, β, γ-CD) as the macrocyclic hosts (Table S5). Therefore, we inferred that the synergistic effect of the spatial confinement of HPCD and the rigid microenvironment of PVA resulted in the ultrahigh phosphorescence quantum yields and ultralong lifetimes.

Mechanism of the efficient blue RTP emission

To explore the RTP emission mechanism of TAD-HPCD/PVA, it is essential to verify the attribution of blue phosphorescence emission first. TAD exhibited a blue emission at 430 nm in the delayed emission spectrum at 78 K in diluted N, N-dimethylformamide, which overlapped well with the RTP emission bands of 0.5 wt% doping PVA films (Fig. S15). It indicated that TAD possessed good dispersion and stability in the PVA matrix at an ultralow doping concentration. Additionally, we performed the ^{1}H NMR spectra to analyze the host-guest binding behaviors between TAD and HPCD. With the addition of HPCD, the proton on the phenyl groups experienced a shift toward the high field, and the apparent binding constant (K_{obs}) of TAD-HPCD was 71 M^{-1} (Fig. 3a, b). Transmission electron microscopy (TEM) revealed TAD-HPCD to be larger nanoparticles (Fig. S16). Furthermore, the Fourier transform infrared (FTIR) spectra of TAD/PVA showed a shorter wavenumber of the O-H group vibration peak located at 3284.68 cm^{-1} than that of TAD-HPCD/PVA located at 3286.77 cm^{-1}. The FTIR spectra of TAB-HPCD/PVA and TAC-HPCD/PVA displayed that the characteristic absorption peaks shifted from 3299.42 cm^{-1} to 3314.86 cm^{-1} and moved from 3285.45 cm^{-1} to 3286.38 cm^{-1}, respectively, as compared with TAB/PVA and TAC/PVA (Fig. S17). The above further indirectly verified that the abundant hydroxyl groups of HPCD could strengthen the hydrogen bond association between the supramolecular assembly and PVA to construct a more rigid network to enhance the RTP emission. These results suggested that in addition to the host-guest inclusion interaction, the hydrogen bonding interactions generated by the abundant hydroxyl

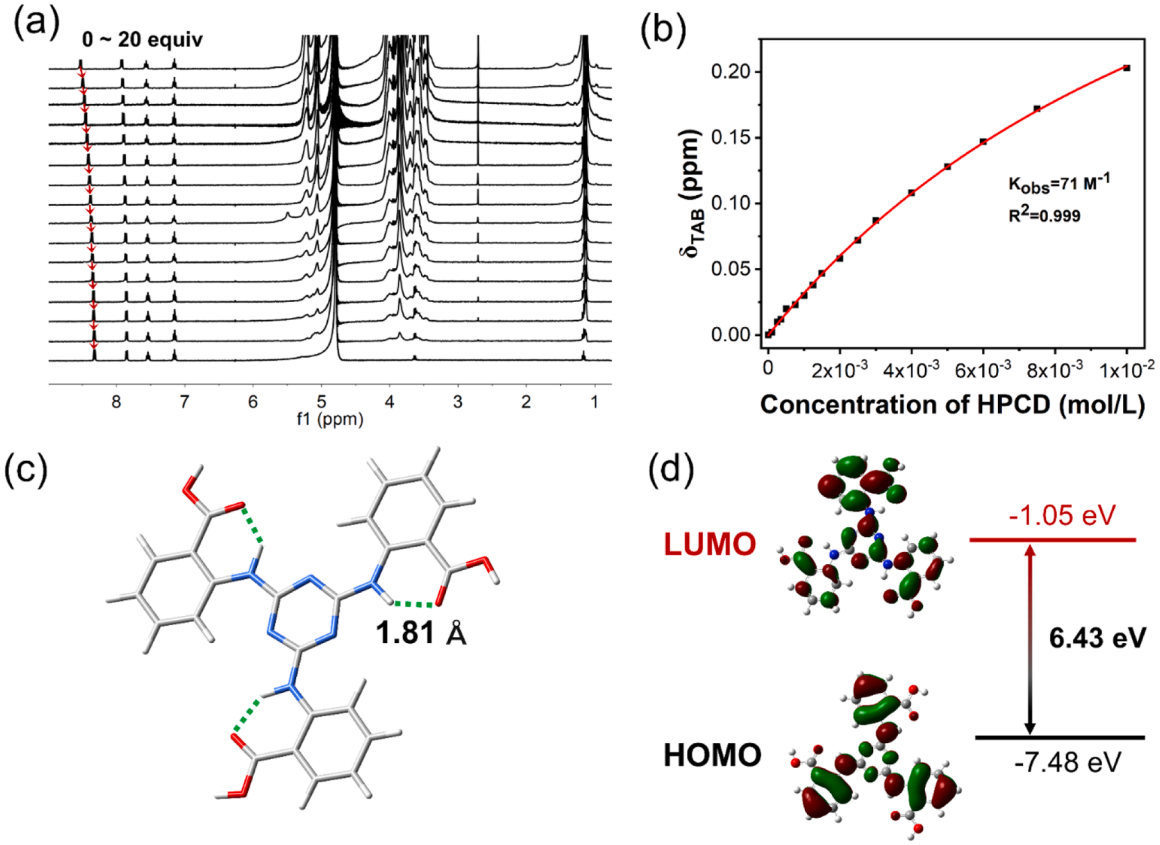

Fig. 3. (a) ^{1}H NMR spectral changes of TAD after adding 0–20 equivalents of HPCD ([TAD] = 5×10^{-4} M, 400 MHz, D_2O, 298 K); (b) The nonlinear least-squares analysis to calculate the association constant between TAD and HPCD; (c) Illustration of IHB of TAD; (d) Energy level distributions of TAD.

groups of HPCD also played an important role in developing the deep-blue phosphorescence.

Given that the triazine moiety was regarded as a phosphorescence-active unit [39], we investigated the luminescence properties of 2-aminobenzoic acid (AD), 3-aminobenzoic acid (AC) and 4-aminobenzoic acid (AB) without the triazine element. Even though they also showed blue phosphorescence emission, the phosphorescent quantum yields and lifetimes of AB-HPCD/PVA (20.17 %, 166.78 ms), AC-HPCD/PVA (2.11 %, 58.75 ms) and AD-HPCD/PVA (11.80 %, 47.96 ms) were all lower than those of triazine derivatives (Fig. S18, S19; Table S6). Therefore, the presence of triazine moiety can promote the blue phosphorescence emission in this system. Subsequently, theoretical calculations further revealed the effect of carboxyl substitution sites on phosphorescence emission. When the -COOH group was substituted at the ortho position of the phenylamine, intramolecular hydrogen bonds (IHB) were found at distances of 1.81 Å. The IHB strengthened the overall structural rigidity of TAD and lowered the molecular vibrational relaxation, thereby suppressing the nonradiative rate [39,40]. Moreover, the HOMO-LUMO distributions of TAB/C/D were evaluated and shown in Fig. 3d and Fig. S20. TAD had the minimum energy gap of 6.43 eV, compared to TAB (6.70 eV) and TAC (6.66 eV). The smaller energy gap can facilitate ISC and then enhance the phosphorescence property [41]. The above may be the reason why TAD-HPCD/PVA displays impressive blue phosphorescence with ultrahigh quantum yield.

Multicolor delayed fluorescence through TS-FRET and SS-FRET

The constructed blue RTP materials with ultralong lifetime are ideal as energy donors to obtain color-tunable organic afterglows through efficient TS-FRET [42]. Two commercialized water-soluble fluorescence dyes (Flu and RhB), were selected as energy acceptors due to the good overlap between their absorption spectra and the phosphorescence spectra of doping PVA systems (Fig. 4a). The delayed emission spectra of Flu/PVA and RhB/PVA showed no characteristic peaks of dyes (Fig. 4d; Fig. S21). However, the delayed spectra of TAD-HPCD@Flu/PVA and TAD-HPCD@RhB/PVA prepared by doping Flu and RhB into 0.5 wt% TAD-HPCD/PVA ([TAD]:[HPCD] = 1:3) showed dual emission peaks of energy donor (430 nm) and energy acceptors (530 nm or 590 nm) in Fig. 4b, e. The delayed fluorescence emissions of TAD-HPCD@Flu/PVA at 530 nm and TAD-HPCD@RhB /PVA at 590 nm enhanced gradually as the ratio of dyes increased. When the molar ratio of TAD:Flu or RhB was 4:1, the optimal delayed fluorescence property of dyes was obtained.

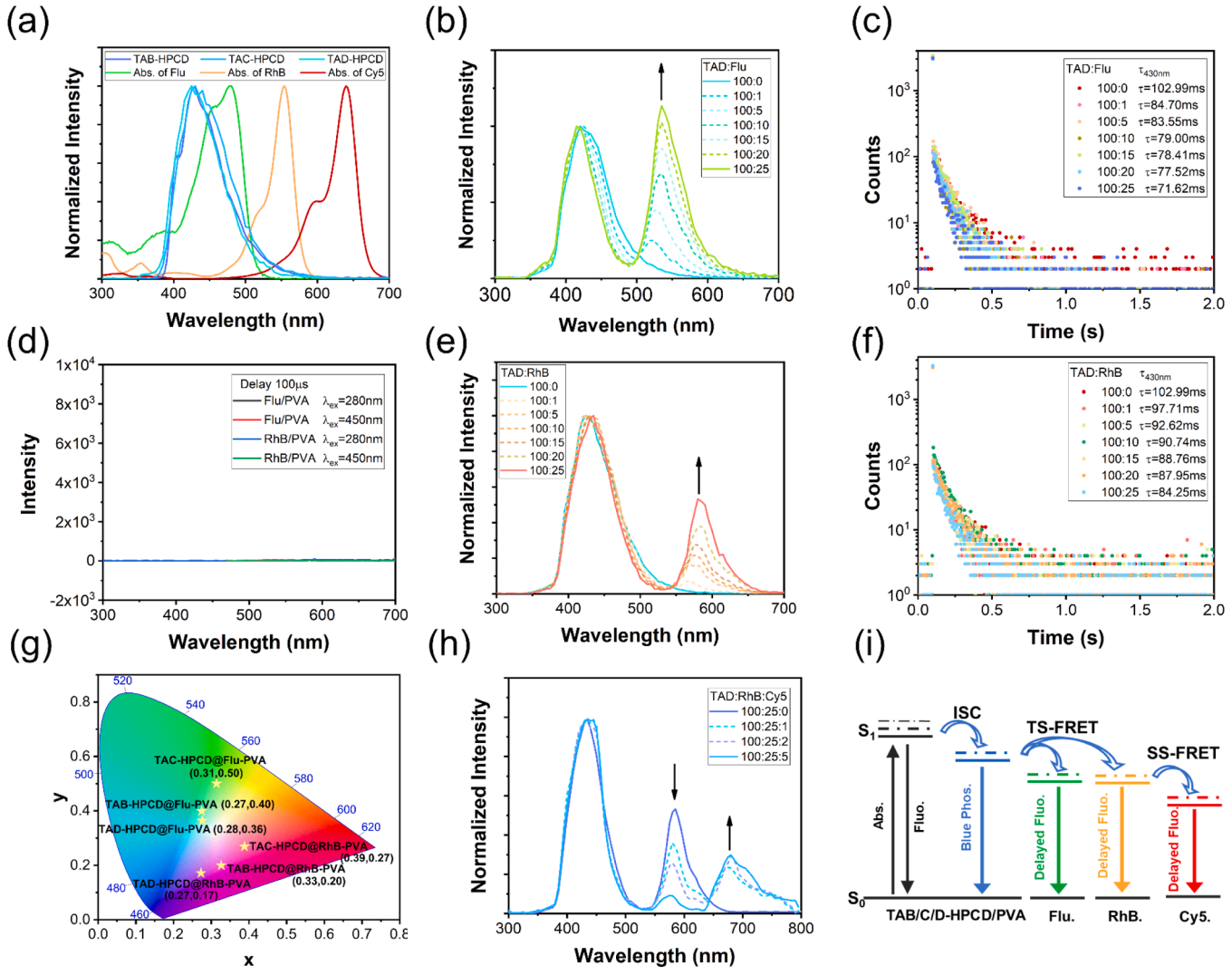

Fig. 4. (a) Normalized phosphorescence spectra of TAB/C/D-HPCD/PVA films (λ_{ex}=280 nm, delayed time=100 μs) and normalized absorption spectra of the energy acceptors Flu, RhB and Cy5; The delayed emission spectra of (b) TAD-HPCD@Flu/PVA, (d) Flu/PVA and RhB/PVA, (e) TAD-HPCD@RhB/PVA and (h) TAD-HPCD@RhB@Cy5/PVA films at different donor/acceptor ratios; Time-resolved decay spectra (recorded at 430 nm) of (c) TAD-HPCD@Flu/PVA and (f) TAD-HPCD@RhB/PVA; (g) CIE chromaticity diagram of TAB/C/D-HPCD@Flu/PVA and TAB/C/D-HPCD@RhB/PVA films according to their phosphorescence spectra; (i) Schematic illustration of TS-FRET and SS-FRET processes.

Meanwhile, the lifetime of the doping film decreased from 102.99 ms (TAD-HPCD/PVA) to 71.26 ms (TAD-HPCD@Flu/PVA) and 84.25 ms (TAD-HPCD@RhB/PVA), corresponding to the energy transfer efficiency (Φ_{ET}) of 30.46 % and 18.19 %, respectively (Fig. 4c, f). Notably, TAD-HPCD@Flu/PVA possessed a delayed fluorescence lifetime of 63.37 ms at 530 nm and TAD-HPCD@RhB/PVA had a lifetime of 65.57 ms at 590 nm (Fig. S22), which further demonstrated the efficient TS-FRET process between the energy donors and acceptors. Similarly, as the doping molar ratio of Flu or RhB increased from 1 % to 25 %, the phosphorescence intensity of TAB-HPCD/PVA gradually reduced, accompanied by a lifetime decrease from 526.03 ms to 180.03 ms (Φ_{ET}=64.49 %) or 246.13 ms (Φ_{ET}=53.21 %), respectively (Fig. S23, S24). The delayed fluorescence lifetimes of TAB-HPCD@Flu/PVA at 530 nm and TAB-HPCD@RhB/PVA at 590 nm were 118.71 ms and 171.76 ms. In addition, TAC-HPCD@Flu/PVA and TAC-HPCD@RhB/PVA also produced the delayed fluorescence emission with lifetimes of 43.37 ms (Φ_{ET}=43.23 %) and 64.81 ms (Φ_{ET}=18.34 %) (Fig. S25, S26). The energy transfer efficiency from TAB/C/D-HPCD/PVA to Flu was higher than that to RhB under the same doping ratio (4:1) and excitation wavelength at 280 nm, which might be due to the better overlap between the Flu absorption and the TAB/C/D-HPCD/PVA emission. Multicolor delayed fluorescence of PVA film has been realized by simply regulating the composition and doping ratio of Flu and RhB through the TS-FRET process. The CIE coordinates showed a significant transition from blue to green and orange regions in Fig. 4g. In particular, multicolor afterglows with tunable lifetimes can be observed by the naked eyes after turning off the 300 nm ultraviolet lamp (Fig. S27).

Considering the light-harvesting system is composed of multiple multicolor components [43,44], we further investigated the potential of cascade energy transfer processes in the doping PVA system. Sulfo-cyanine 5 (Cy5) with 670 nm NIR emission was adopted as the secondary acceptor, of which the absorption spectrum had a better overlap with the emission spectra of TAD-HPCD@RhB/PVA ([TAD]:[RhB]=4:1). With the addition of Cy5, the emission intensity of TAD-HPCD@RhB/PVA at 590 nm decreased, and a new emission peak at 670 nm gradually emerged in Fig. 4h. This result indicated that there was an SS-FRET from the singlet of RhB to the singlet of Cy5. Based on the intensity data of TAD-HPCD@RhB/PVA at 590 nm, the Φ_{ET} was calculated to be 88.53 % when the molar ratio of TAD:RhB:Cy5 was 20:5:1. Besides, both TAB-HPCD@RhB@Cy5/PVA and TAC-HPCD@RhB@Cy5/PVA exhibited NIR delayed fluorescence emission with Φ_{ET} of 90.70 % and 86.79 %, respectively (Fig. S28). The CIE coordinate chart was displayed in the purple region (Fig. S29). Furthermore, we also demonstrated the host-guest binding behaviors between HPCD and dyes by UV–vis spectroscopic experiments, and the binding constants (K_S) of HPCD with Flu, RhB and Cy5 were respectively determined to be 17436 M^{-1}, 9567 M^{-1} and 48111 M^{-1} by the nonlinear least-squares fitting method (Fig. S30). As illustrated in TEM images (Fig. S31), the nanoparticles were gradually enlarged with the addition of fluorescent dyes, which also confirmed the encapsulation of HPCD. Therefore, HPCD is crucial for this supramolecular solid system, not only to enhance the phosphorescence properties of TAB/C/D, but also to confine the dyes to restrain the non-radiative transitions. Flu/PVA, RhB/PVA and Cy5/PVA films possessed nanosecond lifetimes and the delayed emission spectra showed no characteristic peaks of dyes (Fig. S21). TAB/C/D-HPCD@Cy5/PVA did not generate significant delayed fluorescence at 670 nm in the absence of primary acceptors Flu and RhB (Fig. S32). In a word, the cascaded phosphorescence capturing system involving TS-FRET and SS-FRET processes was achieved by simply physically doping dyes into TAB/C/D-HPCD/PVA, thus realizing multicolor delayed fluorescence emissions of primary and secondary energy acceptors and conductively expanding its practical application.

Application in information anticounterfeiting

Considering UV-irradiation-responsive RTP and the tunable organic afterglows of the solid supramolecular PVA system, we explored its potential applications in luminescent display, optical anti-counterfeiting and information encryption. As is well known, the RTP property is sensitive to water [45,46]. First, the delayed emission spectra of TAD-HPCD/PVA were investigated under dry/wet stimuli. The dry TAD-HPCD/PVA film had a phosphorescence emission at 430 nm, but the emission intensity decreased greatly in the presence of water. After the film was heated and dried, the blue phosphorescence peak appeared again. TAB-HPCD/PVA and TAC-HPCD/PVA films also showed similar dry/wet responsiveness. The multiple cycles can be repeated more than 5 times (Fig. S33). Subsequently, the TAB/C/D-HPCD/PVA solutions were written “chemistry” word according to Morse code on the surface of non-fluorescent paper and then dried, as shown in Fig. 5a. The blue pattern can be visible to the naked eye under 300 nm UV light irradiation. However, due to different durations after UV off, only the password “chem” was left. The supramolecular film materials possessed high stability and still had a good luminescent display after two months under ambient conditions. Interestingly, only the password “try” could be observed under UV light when water was applied to the written paper, and all letters disappeared after the UV light was turned off. What counts is that all the information reappeared after drying (Fig. S34). Thus, the 2D information encryption was successfully constructed based on the different afterglow lifetimes and humidity responsiveness.

Moreover, the dyes doped PVA materials can be used for multiple anticounterfeiting encryptions of numbers and painting. Due to the excellent transparency of the initial supramolecular materials, the numbers composed of five encoding materials only showed “12” under sunlight, but emerged “12250618” of green, orange and blue colors upon the UV light irradiation. Ceasing the irradiation, it became “2253” four blue numbers due to the longer afterglow lifetimes (Fig. 5b). Except for the letter and number encryption, an “NKU” school badge pattern was fabricated to enrich the diversity of encryption methods in Fig. 5c. The school badge emitted multicolor fluorescence under 300 nm UV light, which was quite different from the natural color under sunlight. After turning off the light, only the “NKU 1919” pattern remained visible to the naked eye as time went by. The above results proved that the constructed supramolecular system with multicolor afterglow had great potential applications in optical anti-counterfeiting technology.

Conclusion

In conclusion, we have developed an effective approach to construct an amorphous blue phosphorescence supramolecular system based on HPCD and triazine derivatives to achieve multicolor delayed fluorescence. Benefiting from the macrocyclic hydrophobic cavity and abundant hydrogen bonds to inhibit nonradiative transitions of the guests, HPCD can effectively induce and enhance the blue phosphorescence of TAB/C/D. A series of supramolecular assembly films was obtained by further doping TAB/C/D-HPCD nanoparticles into the PVA matrix. Among them, TAD-HPCD/PVA film exhibited the best RTP property with an ultrahigh phosphorescent quantum yield of 71.65 % and a long lifetime of 102.99 ms. Finally, multicolor and lifetime-tunable delayed fluorescences were achieved by doping suitable dyes into supramolecular films through the TS-FRET and SS-FRET, utilizing for coding and decoding, multi-level encryption and luminescent display applications. This work provides an attractive approach for constructing great performance blue phosphorescence supramolecular materials with high phosphorescence efficiency to create cascaded energy transfer systems for achieving multicolor delayed fluorescence.

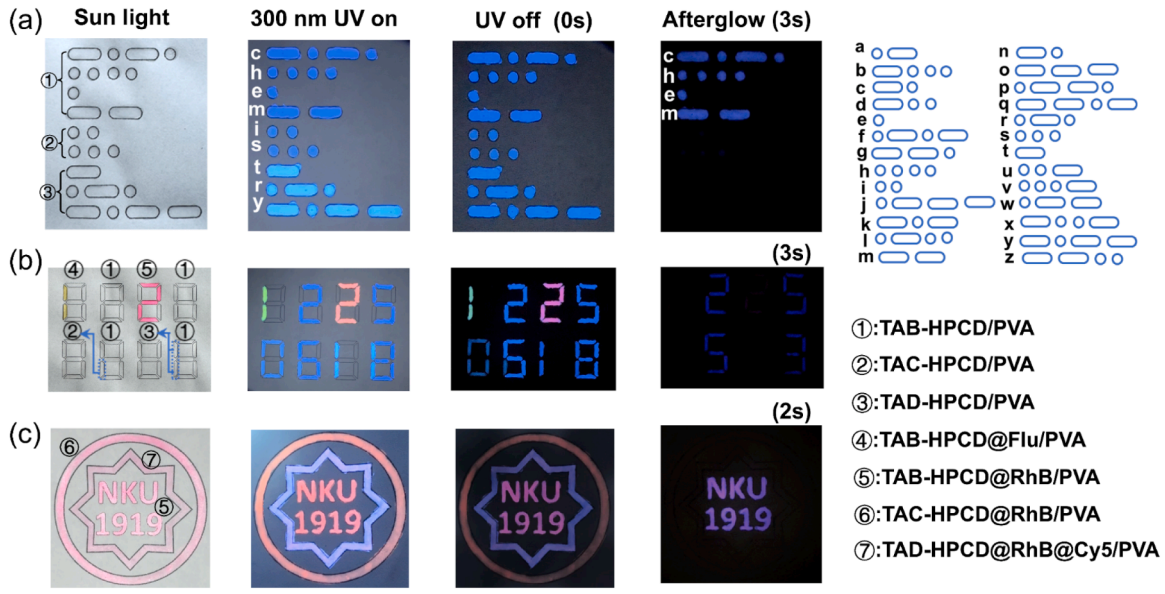

Fig. 5. The applications of different supramolecular assemblies in (a) information encryption of Morse code; (b) Multiple anticounterfeiting encryptions of numbers; (c) Multi-colored drawing of "NKU" school badge pattern.

Experimental section and methods

Materials

All reagents and solvents were purchased from commercial suppliers and used without purification unless specified otherwise. The PVA was purchased from Macklin ($M_W \approx 200{,}000$).

Synthetic route of TAB

4-aminobenzoic acid (3 g, 22 mmol), $NaHCO_3$ (1.5 g, 18.3 mmol) and NaOH (1 g, 25 mmol) were added to deionized water (30 mL). The mixture was stirred at 0 ℃ for 30 minutes. The trimeric cyanamide (1 g, 5.5 mmol) was dissolved in 1, 4-dioxane (10 mL) and then added to the above mixture, which was agitated at 115 ℃ for 24 hours. The resulting solution was acidified with 20 % hydrochloric acid to pH ≈ 3. The formed precipitate (TAB) was filtered and washed with ultrapure water, and then dried in vacuo, to give a yellow powder (Yield: 80 %). TAB: ^{1}H NMR (400 MHz, DMSO-d_6, 298 K) δ: 12.66 (s, 3 H), 9.84 (s, 3 H), 7.98 (d, J = 8.4 Hz, 6 H), 7.89 (d, J = 8.8 Hz, 6 H). ^{13}C NMR (100 MHz, DMSO-d_6, 298 K) δ: 167.56, 164.40, 144.50, 130.52, 124.36, 119.74. HR-ESI-MS: *m/z* calculated for $C_{24}H_{17}N_6O_6^-$: $[TAB-H]^-$, 485.121; found, 485.1209.

Synthetic route of TAC

TAC was synthesized according to TAB with a 72 % yield. ^{1}H NMR (400 MHz, DMSO-d_6, 298 K) δ: 9.51 (s, 3 H), 8.28 (s, 3 H), 8.08 (s, 3 H), 7.57 (d, J = 7.6 Hz, 3 H), 7.39 (t, J = 7.8 Hz, 3 H). ^{13}C NMR (100 MHz, DMSO-d_6, 298 K) δ: 167.87, 164.63, 140.39, 131.76, 129.08, 125.16, 123.44, 121.77. HR-ESI-MS: *m/z* calculated for $C_{24}H_{17}N_6O_6^-$: $[TAC-H]^-$, 485.121; found, 485.1206.

Synthetic route of TAD

2-aminobenzoic acid was prepared according to the literature.[47] TAD was synthesized according to TAB with a 65 % yield. ^{1}H NMR (400 MHz, DMSO-d_6, 298 K) δ: 13.57 (s, 3 H), 10.93 (s, 3 H), 8.64 (d, J = 8.2 Hz, 3 H), 8.02 (d, J = 7.9 Hz, 3 H), 7.61 (t, J = 7.8 Hz, 3 H), 7.13 (t, J = 7.5 Hz, 3 H). ^{13}C NMR (100 MHz, DMSO-d_6, 298 K) δ: 170.06, 164.35, 141.82, 133.99, 131.68, 122.18, 121.32, 117.11. HR-ESI-MS: *m/z* calculated for $C_{24}H_{17}N_6O_6^-$: $[TAD-H]^-$, 485.121; found, 485.1208.

TAB-HPCD supramolecular assembly

TAB (48.64 mg, 0.1 mmol), HPCD (462.30 mg, 0.3 mmol) and K_2CO_3 (72.96 mg) were added to deionized water (5 mL). The aqueous solution was sonicated for 2 h and then lyophilized. The white powder was obtained by further vacuum drying. Similar to the above preparation method, TAC-HPCD and TAD-HPCD have a stoichiometric ratio of host and guest at 3:1.

TAB-HPCD/PVA films

A stirred solution of TAB (0.50 mg, 0.001 mmol), HPCD (4.76 mg, 0.003 mmol) and K_2CO_3 (0.75 mg) in water (0.5 mL), and 10 % PVA water solution 1 mL was added. The mixture was stirred for 2 h. Then drop 0.5 mL of the resulting mixed solution on the tinfoil with a syringe. Heat the tinfoil until the water evaporates (65 ℃, 3 h). TAC-HPCD/PVA and TAD-HPCD/PVA films were prepared according to TAB-HPCD/PVA Film.

TAB-HPCD@Flu/PVA films

Add Flu dye to the TAB-HPCD/PVA donor liquid (n_{TAB}:n_{HPCD} = 1:3, m_{TAB}:m_{PVA} = 1:200) according to different molar ratios. Then, the mixture was ultrasound until completely dissolved. Finally, drop 0.3 mL of the resulting mixed solution on the tinfoil and then heat it at 65 ℃ for 3 h. TAC-HPCD@Flu/PVA, TAD-HPCD@Flu/PVA, TAB-HPCD@RhB/PVA, TAC-HPCD@RhB/PVA and TAD-HPCD@RhB/PVA films were prepared according to TAB-HPCD@Flu /PVA films.

Measurements

^{1}H NMR and ^{13}C NMR spectra were recorded on a Bruker DMX 400 MHz spectrometer at 298 K. High-resolution mass spectra (HRMS) were measured on 6520 Q-TOF LC/MS (Agilent). The UV–vis absorption spectra were recorded in a quartz cell (light path = 1 cm) on a Thermo Fisher Scientific EVO300 PC spectrophotometer with a PTC-348WI temperature controller. Photoluminescence (PL) spectra, absolute quantum yields (QY) and time-correlated decay profiles were documented on Edinburgh Instruments FS5 (Livingstone, UK). The Fourier

transform infrared spectra (FTIR) were processed on Thermofsher Scientific Nicolet iS5. The powder X-ray diffraction (XRD) patterns were recorded by Rigaku SmartLab. The Commission International del' Eclairage (CIE) 1931 chromaticity diagram was determined by FLS1000 software. Transmission electron microscopy (TEM) experiments were accomplished on FEI Tecnai G2 F20 under 200 KV and scanning electron microscopy. The luminescent photos were taken by iPhone 15 Pro max under the irradiation of a UV lamp at room temperature.

CRediT authorship contribution statement

Xiaolu Zhou: Supervision, Software, Methodology. **Qingwen Cheng:** Validation, Supervision, Methodology. **Yu Liu:** Writing – review & editing, Supervision, Resources, Funding acquisition, Conceptualization. **Xuan Zhao:** Writing – review & editing, Writing – original draft, Visualization, Validation, Software, Methodology, Investigation, Formal analysis, Data curation, Conceptualization.

Declaration of Competing Interest

The authors declare that they have no known competing financial interests or personal relationships that could have appeared to influence the work reported in this paper.

Acknowledgments

The authors thank the National Nature Science Foundation of China (NNSFC, Grant Nos. 22131008), China Fundamental Research Funds for the Central Universities, and the Haihe Laboratory of Sustainable Chemical Transformations for financial support.

Appendix A. Supporting information

Supplementary data associated with this article can be found in the online version at doi:10.1016/j.nantod.2024.102561.

Data availability

Data will be made available on request.

References

[1] X.Y. Lou, Y.W. Yang, Adv. Mater. 32 (2020) 2003263.
[2] X.K. Ma, Y. Liu, Acc. Chem. Res. 54 (2021) 3403–3414.
[3] D. Ma, G. Hettiarachchi, D. Nguyen, B. Zhang, J.B. Wittenberg, P.Y. Zavalij, V. Briken, L. Isaacs, Nat. Chem. 4 (2012) 503–510.
[4] Z. Liu, W. Lin, Y. Liu, Acc. Chem. Res. 55 (2022) 3417–3429.
[5] X. Zhao, X. Zhou, W. Xing, Y. Liu, Chem. Commun. 59 (2023) 11516–11519.
[6] J. Zhang, P.X. Ma, Nano Today 5 (2010) 337–350.
[7] B.S.L. Collins, J.C.M. Kistemaker, E. Otte, B.L. Feringa, Nat. Chem. 8 (2016) 860–866.
[8] H. Zheng, L. Fu, R. Wang, J. Jiao, Y. Song, C. Shi, Y. Chen, J. Jiang, C. Lin, J. Ma, L. Wang, Nat. Commun. 14 (2023) 590.
[9] J.D. Badjic, V. Balzani, A. Credi, S. Silvi, J.F. Stoddart, Science 303 (2004) 1845–1849.
[10] S. Garain, B.C. Garain, M. Eswaramoorthy, S.K. Pati, S.J. George, Angew. Chem. Int. Ed. 60 (2021) 19720–19724.
[11] R. Zhang, Y. Chen, Y. Liu, Angew. Chem. Int. Ed. 62 (2023) e202315749.
[12] Z. Liu, H. Chen, M. Tian, X.Y. Sun, Y.X. Li, J. Wu, R.T. Wang, B. Li, C.J. Li, Y. Liu, Aggregate (2024) e627.
[13] Y.F. Zhang, L. Gao, X. Zheng, Z.H. Wang, C.L. Yang, H.L. Tang, L.J. Qu, Y.B. Li, Y. L. Zhao, Nat. Commun. 12 (2021) 2297.
[14] Z.L. Xie, X.Y. Zhang, H.L. Wang, C. Huang, H.D. Sun, M.Y. Dong, L. Ji, Z.F. An, T. Yu, W. Huang, Nat. Commun. 12 (2021) 3522.
[15] S.J. Barrow, S. Kasera, M.J. Rowland, J.D. Barrio, O.A. Scherman, Chem. Rev. 115 (2015) 12320–12406.
[16] X.L. Zhou, X. Bai, F.J. Shang, H.Y. Zhang, L.H. Wang, X.F. Xu, Y. Liu, Nat. Commun. 15 (2024) 4787.
[17] X. Zhao, Y. Chen, X.Y. Dai, W.L. Zhou, J.J. Li, Y. Liu, Adv. Photonics Res. 1 (2020) 2000007.
[18] Y. Wang, P. Wang, W. Li, Z. Lin, Y. Wang, Q. Chen, S. Zhang, Z. He, C. Luo, J. Sun, Nano Today 56 (2024) 102305.
[19] Z.X. Liu, Y. Liu, Chem. Soc. Rev. 51 (2022) 4786–4827.
[20] B. Yang, J. Lin, Y. Chen, Y. Liu, Bioorg. Med. Chem. 17 (2009) 6311–6317.
[21] X.Y. Dai, M. Huo, Y. Liu, Nat. Rev. Chem. 7 (2023) 854–874.
[22] X. Zhao, Y. Chen, X.R. Guan, P.Y. Li, W.L. Zhou, Y. Liu, ChemistrySelect 4 (2019) 13241–13244.
[23] D. Li, Z. j Liu, M.M. Fang, J. Yang, B.Z. Tang, Z. Li, ACS Nano 17 (2023) 12895–12902.
[24] X.L. Zhou, X. Zhao, X. Bai, Q.W. Cheng, Y. Liu, Adv. Funct. Mater. (2024) 2400898.
[25] Z.Y. Zhang, C.Y. Deng, C.C. Shen, R.Y. Xu, X.Z. Wang, Y.H. Wang, B. Ding, B. Li, J. Li, C.J. Li, Chem. Commun. 59 (2023) 11248–11251.
[26] H. Jiang, S. Zhao, Z. Li, L. Chen, H. Mo, X. Liu, Nano Today 56 (2024) 102272.
[27] Z.Z. Li, Q. Yue, Y. He, H.C. Zhang, ACS Appl. Mater. Interfaces 16 (2024) 25415–25421.
[28] D.L. Wang, J.Y. Gong, Y. Xiong, H.Z. Wu, Z. Zhao, D. Wang, B.Z. Tang, Adv. Funct. Mater. 33 (2023) 2208895.
[29] X.W. Liu, W.J. Zhao, Y. Wu, Z.G. Meng, Z.K. He, X. Qi, Y.R. Ren, Z.Q. Yu, B.Z. Tang, Nat. Commun. 13 (2022) 3887.
[30] D.D.S. Pereira, D.R. Lee, N.A. Kukhta, K.H. Lee, C.L. Kim, A.S. Batsanov, J.Y. Lee, A.P. Monkman, J. Mater. Chem. C 7 (2019) 10481.
[31] Z.H. Guan, Z.R. Tang, J.J. Deng, Y.W. Zheng, H.B. Li, X.H. Liu, Adv. Funct. Mater. (2023) 2310198.
[32] Y. Tian, X.B. Tong, J.J. Li, S.Y. Gao, R. Cao, Chin. J. Chem. 40 (2022) 487–492.
[33] S. Xu, W. Wang, H. Li, J.Y. Zhang, R.F. Chen, S. Wang, C. Zheng, G.C. Xing, C. Y. Song, W. Huang, Nat. Commun. 11 (2020) 4802.
[34] S.L. Qu, K. Shen, B.S. Wu, Y.X. He, Z. Zhao, C.Z. Yin, Z.F. An, S.M. Yan, H.F. Shi, Cryst. Growth Des. 23 (2023) 31–36.
[35] H.M. Yu, X.Y. Yu, Y. Chen, Y. Liu, Soft Matter 19 (2023) 3162–3166.
[36] T.T. Li, Y. Zheng, C.Q. Wu, C.Y. Yan, C. Zhang, H. Gao, Q. Chen, K. Zhang, Chin. Chem. Lett. 33 (2022) 4238–4242.
[37] S.D. Xiong, Y. Xiong, D.L. Wang, Y.W. Pan, K.Y. Chen, Z. Zhao, D. Wang, B.Z. Tang, Adv. Mater. 35 (2023) 2301874.
[38] L. Gu, H.F. Shi, C.Y. Miao, Q. Wu, Z.C. Cheng, S.Z. Cai, M.X. Gu, C.Q. Ma, W. Yao, Y.R. Gao, Z.F. An, W. Huang, J. Mater. Chem. C 6 (2018) 226–233.
[39] G.Y. Jiang, Q.Y. Li, A.Q. Lv, L.X. Liu, J.Y. Gong, H.L. Ma, J.G. Wang, B.Z. Tang, J. Mater. Chem. C 10 (2022) 13797–13804.
[40] Y.N. Wang, Y.R. Guo, Z.B. Wu, H.Y. Zhang, C. Wang, G.J. Zhao, J. Mol. Liq. 326 (2021) 115291.
[41] L. Zhou, J.M. Song, Z.Y. He, Y.W. Liu, P. Jiang, T. Li, X. Ma, Angew. Chem. Int. Ed. 63 (2024) e202403773.
[42] F.X. Lin, H.Y. Wang, Y.F. Cao, R.J. Yu, G.D. Liang, H.H. Huang, Y.X. Mu, Z.Y. Yang, Z.G. Chi, Adv. Mater. 34 (2022) 2108333.
[43] Z. Xu, S. Peng, Y.Y. Wang, J.K. Zhang, A.I. Lazar, D.S. Guo, Adv. Mater. 28 (2016) 7666–7671.
[44] Q.W. Cheng, X.K. Ma, X.L. Zhou, Y.M. Zhang, Y. Liu, Small (2023) 2309732.
[45] D. Li, Y.J. Yang, J. Yang, M.M. Fang, B.Z. Tang, Z. Li, Nat. Commun. 13 (2022) 347.
[46] W.Y. Ye, Y.D. Wang, T.Y. Cao, H. Meng, C.L. Wang, B.X. Hu, Z.Y. Gao, C.Q. Wang, Small 19 (2023) 2207403.
[47] Z. Wei, J. Zhang, H. YYang, G. Jiang, Adv. Synth. Catal. 361 (2019) 3694–3697.